Jour. of the KGS, Vol. 23, No. 3. March 2007, pp. 77~88

Elastic-plastic Micromechanics Modeling of Cross-anisotropic Granular Soils: I. Formulation

직교 이방적 사질토의 미시역학적 탄소성 모델링: I. 정식화

Jung, Young-Hoon[1] 정 영 훈
Chung, Choong-Ki[2] 정 충 기

요 지

본 연구에서는 사질토의 탄성 및 탄소성 거동을 모사하기 위한 미시역학 기반의 구성 모델을 개발하였다. 개발 모델은 접촉 방향의 공간 분포를 통계적으로 처리한 조직 이방성, 응력비에 따른 조직 이방성의 변화, 간극비 변화에 따른 접촉점 수의 변화, 그리고 미시적 탄성-탄소성 접촉 강성을 고려하였다. 금속 재료에 대한 시험결과를 이용하여 미시적 탄소성 접촉 강성 모델을 수직 접촉력과 입자의 항복 접촉력에 대한 거듭제곱 함수의 형태로 유도하였다. 모델 변수를 정량적으로 평가하기 위해 직교 이방 탄성 계수의 근사식을 유도하였다.

Abstract

A micromechanics-based model to simulate the elastic and elastic-plastic behavior of granular soils is developed. The model accounts for the fabric anisotropy represented by the statistical parameter of the spatial distribution of contact normals, the evolution of fabric anisotropy as a function of stress ratio, the continuous change of the co-ordination number relating to the void ratio, and the elastic and elastic-plastic microscopic contact stiffness. Using the experimental data for metallic materials, the elastic-plastic contact stiffness is derived as a power function of the normal contact force as well as the contact force initiating the yielding of contact bodies. To quantitatively assess microscopic model parameters, approximate solutions of cross-anisotropic elastic moduli are derived in terms of the micromechanical parameters.

Keywords : Constitutive modeling, Elastic-plastic behavior, Granular soils, Micromechanics

1. Introduction

Recently, a number of sophisticated constitutive models (e.g. Einav and Puzrin 2004; Pestana et al. 2002; Stallebrass and Taylor 1997) based on the traditional continuum mechanics have been developed to incorporate plenty of new information on soil behavior. Data showing severe nonlinearity in stress-strain responses force a new elastic-plastic model into employing a number of yield surfaces as well as increasing the number of model parameters. Even in the so-called simplified pseudo-elastic model (e.g. Jung et al. 2004; Puzrin and Burland 2000), higher-order nonlinear equations are inevitable to match its simulation with realistic soil responses. Unfortunately,

1 Member, Post-doctoral fellow, Dept. of Civil and Env. Engrg., Northwestern Univ., 2145 Sheridan Rd. Rm. AG 50, Evanston, IL 60208, U.S.A., j-young-hoon@northwestern.edu, Corresponding Author
2 Member, Prof., School of Civil and Environment Engrg., Seoul National Univ., San 56-1, Shillim-dong, Kwanak-gu, Seoul 151-742, Korea

such great effort based on the continuum mechanics does not guarantee that one can simulate a realistic nonlinear response of soils in the whole range of deformation. Obviously, a simple reason contributes to unsatisfactory performance of the conventional continuum-based soil models: soil is not a continuum material but a particulate material.

Micromechanics theory, in which the interaction among contacts of particles at the micro scale is being scaled up to calculate the macroscopic deformation, is a viable alternative to the traditional continuum mechanics in soil modeling. For the last two decades, two different types of micromechanics approaches—discrete element method and microstructural continuum mechanics—have been used to simulate the nonlinear behavior, especially of granular soils. The discrete element method (Cundall and Strack 1979), in which the interaction between two particles is computed explicitly to retrieve the macroscopic stress-strain data, usually requires a new workspace in computation and interpretation, whereas the microstructural continuum mechanics incorporates a conventional form of incremental stress-strain relationships in the calculation. Currently, significant efforts in the microstructural continuum mechanics (hereinafter called the micromechanics) have been devoted to the interpretation and simulation of various aspects of nonlinear responses in granular soils. Theoretical micromechanics analysis on the soil elasticity has made progress beyond the classical studies on regular packing structures. By using homogenization techniques, Chang et al. (1995) and Liao et al. (2000) proposed the analytical solutions of elastic moduli for a random packing assembly with the anisotropic fabric and the nonlinear contact stiffness, respectively.

The primary focus of this paper is to develop the micromechanics-based elastic-plastic constitutive model to simulate the nonlinear cross-anisotropic behavior of granular soils. The model accounts for the fabric anisotropy represented by the statistical parameter of the spatial distribution of contact normals, the evolution of fabric anisotropy as a function of stress ratio, the continuous change of the co-ordination number relating to the void ratio, and the elastic and elastic-plastic microscopic contact stiffness. The microscopic behavior in a single contact point is thoroughly examined for the various states of contact geometries to find the best expression of the microscopic contact stiffness accounting for the naturally generated heterogeneity of the contact surface of granules. In addition, the approximate analytical solutions of cross-anisotropic elastic moduli and the simple linear relationship between the degree of fabric anisotropy and the stress ratio are provided to finely calibrate the microscopic parameters in the model.

2. Micromechanics Formulation

The computational scales of the micromechanics approach can be categorized into three different levels: (i) the macroscopic level in which for an assembly of particles the boundary stresses and strains are related by integrating all the information from the lower levels, (ii) the inter-contact level in which the contact density and the orientation of each contact are statistically described, and (iii) the microscopic level in which a law relating the force acting on a particular orientation of the contact plane to the corresponding displacement is established.

2.1 Notation and Main Assumptions

As shown in Fig. 1, two different reference frames—the global (x_1 - x_2 - x_3) and local (s - t - n) reference frames—

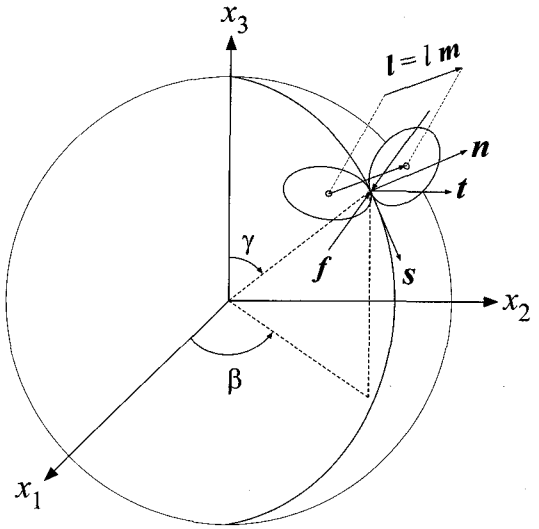

Fig. 1. Global and local coordinate systems in the unit sphere

are used to describe the macroscopic and microscopic behaviors in a separate way. Any nonscalar quantity describing the microscopic response at a single contact point is denoted by ${}^{g}\mathbf{A}$ in the local reference frame and $\mathbf{A}$ in the global reference frame. The transformation of the quantity from the local reference frame to the global frame can be done by defining the rotation matrix, $\mathbf{R}$, as:

$$\mathbf{R}=\begin{bmatrix} s_1 & t_1 & n_1 \\ s_2 & t_2 & n_2 \\ s_3 & t_3 & n_3 \end{bmatrix}=\begin{bmatrix} \cos\gamma\cos\beta & -\sin\beta & \sin\gamma\cos\beta \\ \cos\gamma\sin\beta & \cos\beta & \sin\gamma\sin\beta \\ -\sin\gamma & 0 & \cos\gamma \end{bmatrix} \quad (1)$$

where γ and β represents the angles in the global reference frame as indicated in Fig. 1, and n_i, s_i, and t_i denote the component of the unit vectors, $\mathbf{n}$, $\mathbf{s}$, and $\mathbf{t}$ corresponding to the orthogonal axes of the local reference frame, respectively. Thus, a quantity $\mathbf{A}$ in the global reference frame will be transformed by ${}^{g}\mathbf{A}=\mathbf{R}^{\mathrm{T}}\mathbf{A}$ in the local reference frame.

As shown in Fig. 1, the branch vector, $\mathbf{l}$, represents the vector connecting the centroids of two contacting granules. The branch vector for the c-th contact point can be expressed by

$$\mathbf{l}^{c}=l^{c}\mathbf{m}^{c} \quad (2)$$

where l and $\mathbf{m}$ are the branch length and unit branch vector, respectively. For the finite number N of contacts within the assembly, a fabric tensor, F_{ij}, is given by (Oda et al. 1982),

$$F_{ij}=\frac{1}{V}\sum_{c=1}^{N} l_i^{c} m_j^{c} \quad (3)$$

where N is the total number of contacts, V is the volume of the particle assembly. A transition to continuously distributed branch vectors can be achieved by introducing an orientation distribution function (ODF), $E(\mathbf{m})$, which gives the relative density of the branches whose vectors have the same orientation (γ, β) in the unit sphere, Ω. Assuming that the distribution of branch lengths is continuous and also uncorrelated with that of branch vectors, the fabric tensor can be rewritten as,

$$F_{ij}=\frac{N}{V}\int_{\Omega} l_i m_j E(\mathbf{m})d\Omega=\frac{N}{V}\bar{l}\int_{\Omega} m_i m_j E(\mathbf{m})d\Omega=\frac{N}{V}\bar{l}\left\langle m_i m_j\right\rangle \quad (4)$$

where $\bar{l}$ is the overall average of branch lengths. It is noted that the use of the mean value of branch length distribution, in principle, resorts to the assumption on an ideal assembly with equal-sized spheres. For further simplification, it is assumed that (i) the shape of particles is spherical, thus replacing the branch vector, $\mathbf{m}$, with the contact normal, $\mathbf{n}$, and (ii) the distribution of branch lengths are represented by $\bar{l}$ which is equal to the mean diameter of particles, d_g, for the assembly of equal-sized spherical particles. Detailed discussion on the fabric tensor of the polydisperse granular materials can be found in Madadi et al. (2004).

The angle brackets in the last term of Eq. (4) denotes the weighted average operator using the continuous function of $E(\mathbf{m})$. Thus, a quantity within the angle brackets represents the microscopic quantity at the contacts with the same direction of $\mathbf{m}$ prior to considering the relative contact density with its orientation. It is also worth noting that herein the term 'microscopic' means the averaged micro-directional response over the contacts sharing a given direction of the contact normal, rather than the individual response at each contact point.

The orientation distribution function, $E(\mathbf{n})$, expressed by the angle γ and β, needs to satisfy

$$\int_{\Omega} E(\mathbf{n})d\Omega=\frac{1}{4\pi}\int_{0}^{2\pi}\int_{0}^{\pi} E(\gamma,\beta)\sin\gamma d\gamma d\beta=1 \quad (5)$$

where $E(\gamma, \beta)\sin\gamma$ is the relative number of contacts with orientation (γ, β). According to Chang et al. (1989), the function of $E(\mathbf{n})$ for the cross-anisotropic material can be expressed by the second-order spherical harmonics with the symmetry of the vertical axis in the global reference frame, x_3, (i.e. the function of γ), as:

$$E(\mathbf{n})=E(\gamma)=\frac{3(1+a\cos 2\gamma)}{(3-a)} \quad (6)$$

where a is the so-called 'degree of fabric anisotropy' ($-1 < a < 1$) which controls the shape of the angular distribution of contact normals.

The contact density, ρ_c, which denotes the average number of contacts per unit volume, can relate to the void ratio for the assembly of equal-sized particles by adopting the published empirical relationship (Chang et al. 1991; Mehrabadi et al. 1982) as:

$$\rho_c = \frac{N}{V} = \frac{3c_n}{\pi d_g^3(1+e)} = \frac{3(13.28-8e)}{\pi d_g^3(1+e)} \tag{7}$$

where c_n is the co-ordination number indicating the mean number of contacts per particle, d_g is the mean diameter of particles, and e is the void ratio. As noted by Nicot and Darve (2006), a single relationship between the void ratio and the co-ordination number used in Eq. (7) may not be valid after the failure peak for dense materials where the dilatancy induces the major change in the void ratio without changing the co-ordination number. Herein, we limit our discussion to the non-dilative deformation of granular soils. This is also necessary for interpreting the experimental data because the empirical correlation between macroscopic elastic moduli and principal stresses, which is essential to describe the experimental soil elasticity in this research, no longer apply when the dilatancy of the specimen occurs (Kuwano and Jardine 2002; Yu and Richart 1984). As the void ratio changes during loading, the value of co-ordination number keeps updated in the incremental formulation of the micromechanics constitutive model.

2.2 Relationship Between Microscopic and Macroscopic Quantities

Following the well-established average procedure based on principle of virtual work (Chang et al. 1989; Christoffersen et al. 1981; Love 1927; Mehrabadi et al. 1982), the macroscopic stress tensor, σ_{ij}, can be expressed in terms of the microscopic contact forces, f_i, as:

$$\sigma_{ij} = \rho_c d_g \int_\Omega f_i n_j E(\mathbf{n}) d\Omega \tag{8}$$

Instead of the kinematic assumption of the uniform deformation field, the average macroscopic strain tensor, ε_{ij}, derived from a least square minimization of the mean displacement field (Emeriault and Chang 1997; Liao et al. 1997), is employed. The expression of ε_{ij} in terms of the contact displacement, δ_i, is given by,

$$\varepsilon_{ij} = \rho_c \int_\Omega \delta_i n_k F_{jk}^{-1} E(\mathbf{n}) d\Omega \tag{9}$$

where F_{ij}^{-1} is the inverse of the fabric tensor, F_{ij}, in Eq. (4).

The macroscopic stress-strain relationship can be derived in either of two different approaches: one is the kinematic hypothesis where the stress-strain relationship is derived from the average stress in Eq. (8) along with the assumption of the uniform deformation field, given by

$$\delta_i = \varepsilon_{ji} l_j = \varepsilon_{ji} d_g n_j \tag{10}$$

Another approach is the static hypothesis where the derivation of the stress-strain relationship starts from the average strain definition in Eq. (9), followed by the static hypothesis equation (Chang et al. 1995; Chang and Gao 1996; Liao et al. 2000; Liao et al. 1997) defining the mean contact force on a given contact orientation as:

$$f_i = \sigma_{ij} n_k F_{jk}^{-1} \tag{11}$$

Herein, the static hypothesis approach is used because the static hypothesis equation accounts for the effect of strain fluctuation in a granular material (Liao et al. 1997) and provides the local magnitude of the contact force directly to the microscopic contact stiffness. In order to match the empirical correlation of the elastic moduli, the incremental form of the elastic constitutive equation is derived.

Differentiation of Eq. (9) yields the incremental macroscopic strain as

$$\dot{\varepsilon}_{ij} = \rho_c \int_\Omega \dot{\delta}_i n_k F_{jk}^{-1} E(\mathbf{n}) d\Omega + \rho_c \int_\Omega \delta_i \dot{n}_k F_{jk}^{-1} E(\mathbf{n}) d\Omega + \rho_c \int_\Omega \delta_i n_k \dot{F}_{jk}^{-1} E(\mathbf{n}) d\Omega + \rho_c \int_\Omega \delta_i n_k F_{jk} \dot{E}(\mathbf{n}) d\Omega \tag{12}$$

As inferred by Eq. (12), a full description of the macroscopic responses requires the proper formulations including (i) the elastic and plastic micro-macro responses

for the condition of the fixed packing structure (i.e. first term in Eq. (12)), and (ii) the change of packing structure or the fabric evolution (i.e. terms for $\dot{n}_i$, $\dot{F}_{ij}^{-1}$, and $\dot{E}(\mathbf{n})$). The elastic-plastic micro-macro response can be taken into account by extending the local contact stiffness to the elastic-plastic model. However, the rigorous formulations related to the change of packing structure may be difficult to derive because $\dot{n}_i$, $\dot{F}_{ij}^{-1}$ and $\dot{E}(\mathbf{n})$ correlate to each other in the static hypothesis formulation and, in principle, results from the particle rotation and spin as well as the tangential elastic-plastic displacement in the contact planes. Within the kinematic assumption of the uniform deformation field, Darve and Nicot (2005) and Nicot and Darve (2006) provided the in-depth platform for the incrementally nonlinear formulation of the complete micromechanics model considering the fabric evolution. In an alternative way, the change of packing structure, $\dot{E}(\mathbf{n})$, can be investigated exclusively by tracing possible differences between the elastic moduli measured in the experiment and the micromechanics-based elastic stiffness during loading. Herein, we employed the alternative method to measure the evolution of fabric as will be shown in the subsequent paper. Therefore, the further formulation in the micromechanics model will focus on the incremental formulation of stress-strain relationship via the elastic-plastic contact stiffness. It is assumed that the statue of the fabric in an increment is constant; however, the state of soil fabric expressed by $E(\mathbf{n})$ keeps updated as the stress changes during loading.

For a given state of the fabric, Eq. (12) yields the incremental strains as

$$\dot{\varepsilon}_{ij} = \rho_c \int_{\Omega} \dot{\delta}_i \, n_k F_{jk}^{-1} E(\mathbf{n}) d\Omega \tag{13}$$

Replacing $\dot{\delta}_i$ with the incremental contact force, $\dot{f}_i$, yields

$$\dot{\varepsilon}_{ij} = \rho_c \int_{\Omega} (K_{ip}^{ep})^{-1} \dot{f}_p n_k F_{jk}^{-1} E(\mathbf{n}) d\Omega \tag{14}$$

where K_{ip}^{ep} represents the elastic-plastic contact stiffness tensor, which relates the incremental contact force to the incremental contact displacement as:

$$\dot{f}_i = K_{ij}^{ep} \dot{\delta}_j \tag{15}$$

By substituting the incremental form of Eq. (11) for the fixed packing structure into Eq. (14), the macroscopic compliance tensor, C_{ijkl}^{el}, can be formulated as:

$$\dot{\varepsilon}_{ij} = C_{ijkl} \dot{\sigma}_{kl} = \left[\rho_c \int_{\Omega} (n_m F_{lm}^{-1})(K_{ik}^{ep})^{-1} (n_n F_{jn}^{-1}) E(\mathbf{n}) d\Omega \right] \dot{\sigma}_{kl} \tag{16}$$

Adopting the conventional notion of elastic-plastic strain decomposition, the elastic strain-stress relationship can be derived by

$$\dot{\varepsilon}_{ij}^{el} = C_{ijkl}^{el} \dot{\sigma}_{kl} = \left[\rho_c \int_{\Omega} (n_m F_{lm}^{-1})(K_{ik}^{el})^{-1} (n_n F_{jn}^{-1}) E(\mathbf{n}) d\Omega \right] \dot{\sigma}_{kl} \tag{17}$$

where $\dot{\varepsilon}_{ij}^{el}$ is the elastic strain increment, C_{ijkl}^{el} is the macroscopic elastic compliance tensor, and K_{ip}^{ep} is the microscopic elastic contact stiffness. A simple numerical integration method is used to approximate the integral in Eq. (17), while some researchers (e.g. Bazant et al. 2000; Fang 2003; Hicher and Chang 2005) have introduced the optimal Gaussian formula to reduce computational time.

3. Nonlinear Contact Stiffness Model

The contact stiffness model in the microscopic level defines the relationship between the contact force and contact displacement. Assuming no coupling effect between the elastic responses in the normal and that in the tangential directions on a contact plane, the elastic contact stiffness in the global reference frame, K_{ij}, can be related to that in the local reference frame, ${}^{g}K_{ij}$, as follows:

$$K_{ij} = {}^{g}K_{11} s_i s_j + {}^{g}K_{22} t_i t_j + {}^{g}K_{33} n_i n_j = {}^{g}k_n n_i n_j + {}^{g}k_r (s_i s_j + t_i t_j) \tag{18}$$

where ${}^{g}K_n$ and ${}^{g}K_r$ are the normal and tangential contact stiffnesses in the local reference frame, respectively.

3.1 Geometry of Contact Surfaces

The area of contact under an incipient contact force

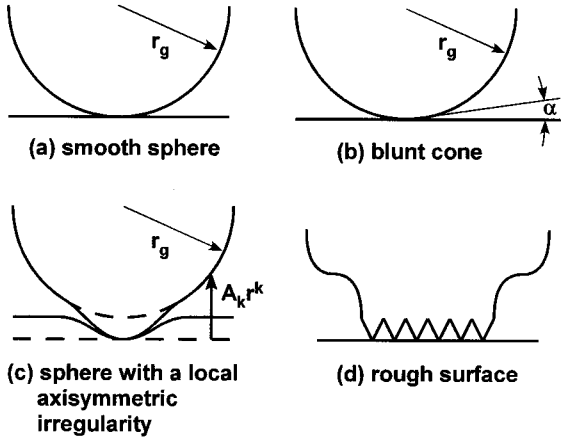

Fig. 2. Geometry of contact surface

and the distribution of the pressure acting on the contact area determine the contact stiffness. Soil particle, generally, has a significant order of irregularity on its geometry of surfaces. Thus, the severe idealization of the geometry of contact surface is inevitable to measure the area of contact and the distribution of contact pressure.

In the theory of tribology, the idealized geometry for the axisymmetric contact surface can be categorized as: (i) smooth sphere, (ii) blunt cone, (iii) sphere with a local axisymmetric irregularity, and (iv) rough surface with the numerous irregularities, as illustrated in Fig. 2. While the assumption of smooth sphere leads to severe restriction to simulate the real contact phenomena, the expressions established for this geometry such as the Hertzian contact (Hertz 1882) serve as a basic formulation for the contact force-displacement relationship for the other contact geometries. For the contact problems of the granular soils, it may be reasonable that the geometry of contact surfaces is idealized as the rough surface for the larger particles or the sphere with a local axisymmetric irregularity for the smaller particles.

3.2 Elastic Contact Stiffness

The normal elastic contact stiffness is formulated as a general form based on the classical Hertz theory for the contact between two smooth spheres, as:

$$ {}^{g}k_n^{el} = c_n({}^{g}f_n / f_{ref})^{\alpha_n^{el}} \tag{19} $$

where ${}^{g}f_n$ is the normal contact force in the local reference frame, f_{ref} is the reference force (1 kN), used as a normalizing constant, c_n^{el} and α_n^{el} are the material constants which relate to the geometry of contact and material properties. For instance, the Hertz's model yields

$$ c_n^{el} = [3r_c G_g^2/(1-\nu_g)^2]^{1/3} \quad \text{and} \quad \alpha_n^{el} = 1/3 \tag{20} $$

where r_c is the radius of curvature of the contact surface, G_g and ν_g are the elastic shear modulus and the Poisson's ratio of particles, respectively. The general form of the normal contact stiffness given in Eq. (19) can be adopted for various contact conditions, which do not obey the ideal condition in the Hertz's theory, such as the contact of a blunt cone on the plane (Goddard 1990) and the contact between the rough surfaces (Yimsiri and Soga 2000). For the contact in the spheres with a local axisymmetric irregularity, which closely simulates the realistic contact behavior in the granular soils, Jäger (1999) shows that the exponent in the equation of the normal contact stiffness (e.g. α_n^{el} in Eq. (19)) is greater than 0.5 when the surface has an acute peak and this value decreases as the irregularity becomes flatter as shown in Fig. 3.

The tangential elastic contact stiffness is also formulated as a general form based on the Mindlin's model without partial slippages (Johnson 1985; Mindlin 1949), given by

$$ {}^{g}k_r^{el} = c_r^{el}\,{}^{g}k_n^{el} \tag{21} $$

where c_r^{el} denotes the proportional factor, which relates to the bulk elastic distortion. Herein, the Mindlin's tangential contact stiffness model is adopted, thus leading to

$$ c_r^{el} = 2(1-\nu_g)/(2-\nu_g) \tag{22} $$

In summary, the contact stiffness model in Eqs. (19) and (21) requires three parameters of c_n^{el}, α_n^{el}, and c_r^{el}. By referring to published values of the Poisson's ratio for a specific mineral type of particles, one can easily determine c_r^{el} based on Eq. (22). However, determination of c_n^{el} and α_n^{el} is not straightforward because these parameters relate not only to mechanical properties of

particles but also to geometries of the contacts.

3.3 Elastic-plastic Contact Stiffness

The solutions for the contact in the elastic bodies remain valid until the applied load is sufficiently large so as to initiate plastic deformation. When the internal stress at a specific point within the contact body reaches the yield strength of material, the yielding will be initiated. However, the plastic zone at the initial yielding stage is very small and fully contained by the material which remains elastic. In this circumstance, the material displaced by the indenter is accommodated by an elastic expansion of the surrounding elastic solid. Thus, the elasticity of material plays an important part in the early stage of the plastic indentation process. As the indentation becomes more severe, the plastic zone breaks out to the free surface and the material reaches a fully plastic state.

The three ranges of loading: purely elastic, elastic-plastic and fully plastic are the common feature of most engineering materials. The early two stages of contact loading (i.e. purely elastic and elastic-plastic stages) are likely to appear in the perfect plastic or brittle materials including the granular soils. For the strain-hardening material such as steel and bronze, the plastic flow or straining continuously occurs in the fully plastic state with the increasing contact pressure. However, the additional resisting of the strain-hardening material at the fully plastic stage cannot be expected in the brittle material. A sudden drop of stiffness or an unlimited plastic flow will occur and the brittle particles will be crushed.

If the contact force acting on a single contact point is below a specific value which yields the crushing or fully plastic failure of the particle, it could be postulated that the elastic-plastic contact behavior of granular soils exhibits the same response in the metallic materials. It is also expected that the response of granular soils at the elastic-plastic stage involves the irrecoverable volumetric compression associated with progressive crushing of the materials. If this hypothesis is correct, one can formulate the elastic-plastic contact stiffness of granular soils using the experimental data on the force-displacement relations at the elastic-plastic stage of metallic materials.

Johnson (1985) summarized the experimental data on the normalized force-displacement relationship in the metallic material for the case of penetration of a spherical indenter into an elastic-plastic half-space, as shown in Fig. 4. According to Adams and Nosonovsky (2000), both the Tresca and the von Mises theories predict the onset of yielding induced by the spherical indenter when

$$f_Y = \frac{\pi r_c^2 (1-\nu_g)^2}{8G_g^2} Y^3 \quad \text{and} \quad \delta_Y = \frac{\pi r_c (1-\nu_g)^2}{4G_g^2} Y^2 \tag{23}$$

where f_Y represents the maximum contact force to initiate yielding of the contact, δ_Y is the corresponding displacement at the onset of yielding, r_c is the radius of curvature at the contact point, and Y is the yield stress of material. Johnson (1985) reported that the material reaches the fully plastic stage when $f_n = 400 f_Y$ for the metallic materials. Accordingly, the experimental data on the limited range of $1 \leq f_n / f_Y \leq 400$ can be used to formulate the elastic-plastic contact stiffness.

In this study, it is assumed that the normalized force-displacement relationship at the elastic-plastic stage can be expressed by an exponential function similar to the elastic case, given by

$$\frac{{}^g f_n}{f_Y} = \left(\frac{{}^g \delta_n}{\delta_Y} \right)^\theta \quad \text{and} \quad \frac{{}^g \delta_n}{\delta_Y} = \left(\frac{{}^g f_n}{f_Y} \right)^{1/\theta} \tag{24}$$

where θ is the material constant governing the power

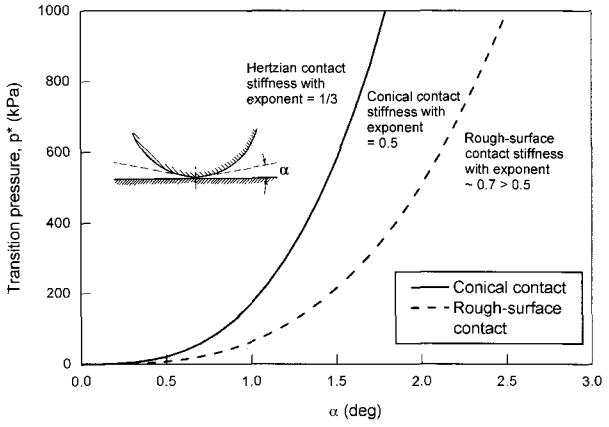

Fig. 3. Transition pressure plotted against α for the FCC packing of quartz

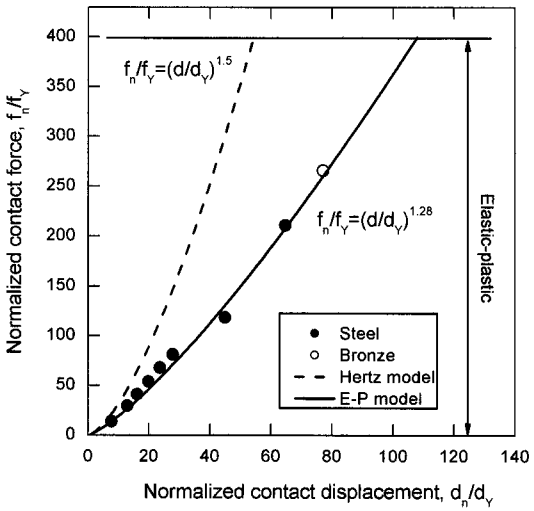

Fig. 4. Normalized force-displacement relationship at the elastic-plastic stage

relationship in the elastic-plastic contact deformation. The interpolation over the experimental data given in Fig. 4 indicates that the value of exponent $\theta = 1.28$. By differentiating Eq. (24), the elastic-plastic contact stiffness can be expressed as

$$ {}^{g}k_n^{el} = \frac{d\,{}^{g}f_n}{d\,{}^{g}\delta_n} = \theta \frac{f_Y}{{}^{g}\delta_Y}\left(\frac{{}^{g}f_n}{f_Y}\right)^{(\theta-1)/\theta} = \frac{\theta (f_Y)^{1/\theta}}{\delta_Y}\left({}^{g}f_n\right)^{(\theta-1)/\theta} \quad (25) $$

For $\theta = 1.28$, the exponent of elastic-plastic contact stiffness $(\theta - 1)/\theta = 0.22$. In the elastic-plastic contact, the pressure distribution of plastic indentation spreads over larger area than that in the Hertz contact model. The response in the elastic-plastic contact of spherical indenter could represent the responses for other contact geometries based on the observation of Samuels and Mulhearn (1956) and Mulhearn (1959), who reported that the subsurface displacements produced by any blunt indenter (cone, sphere or pyramid) are approximately radial from the point of first contact, with roughly hemi-spherical contour of the equal strains. Herein, the generalized elastic-plastic contact stiffness is used given by

$$ {}^{g}k_n^{ep} = c_n^{ep}\left({}^{g}f_n / f_{ref}\right)^{\alpha_n^{ep}} \quad (26) $$

where c_n^{ep} is the material constant relating to f_Y, δ_Y, and θ as introduced in Eq. (25), and α_n^{ep} is the exponent with the value of 0.22 based on the experimental data for the metallic materials, and f_{ref} is the normalizing constant (1 kN).

Considering the origin of friction induced by plastic deformation of contact, Mindlin's model including micro-slip could be regarded as one of the idealized formulations of the tangential contact stiffness of elastic-plastic bodies. Herein, we employ a function that approximates the expressions of Mindlin and Deresiewicz (1953) for the tangential contact stiffness as follows:

$$ {}^{g}k_r^{ep} = {}^{g}k_r^{0}\left(1 - \frac{{}^{g}f_r}{{}^{g}f_n \tan\phi_m}\right)^{\alpha_r^{ep}} = c_r^{ep}\,{}^{g}k_n^{ep}\left(1 - \frac{{}^{g}f_r}{{}^{g}f_n \tan\phi_m}\right)^{\alpha_r^{ep}} \quad (27) $$

where ${}^{g}k_r^{0}$ is the initial tangential stiffness, and α_r^{ep} is a fixed parameter usually set to 1/3 to agree with Mindlin's theory. The parameter c_r^{ep} represents the distortion during tangential loading on the elastic-plastic bodies, which is certainly similar to c_r^{el} because most part of contact bodies still deform elastically even under the plastic indentation and the tangential loading. Thus, it is assumed that the value of c_r^{el} is the same as that of c_r^{el}.

For the general case of contact geometry, the value of α_r^{ep} is different from 1/3. Walton and Braun (1986) reported that experimental measurements of initial displacements of frictional forces acting between metals in contact of non-spherical bodies produce force deflection curves with a more gradual change in slope, as would be produced with a larger value for the exponent α_r^{ep}. However, specific ranges of the exponent have not been reported yet in the literature. Thus, one can only expect that in the contact with the irregular surface of granular soils the value of α_r^{ep} would be greater than 1/3.

4. Approximate Solutions of Cross-anisotropic Elastic Moduli

A constitutive equation based on the micromechanics theory requires a relatively small number of model parameters. However, the determination of such parameters, especially for the microscopic contact stiffness, is not straightforward. One of the reasonable ways to determine such parameters is to compare the closed-form solutions

of macroscopic elastic moduli expressed by these parameters to the experimental data obtained in the macroscopic scale. However, rigorous solutions accounting both for the nonlinear contact stiffness and the anisotropic fabric cannot be derived (Emeriault and Cambou 1996). Herein, instead of developing a rigorous form of equations, the approximate approach to obtain closed-form solutions is attempted.

If a soil assembly consisting of the spherical particles with the symmetric distribution of contact orientations is subject to the isotropic stress of σ_0, Eq. (11) becomes

$$f_1 = \sigma_0 n_1 F_{11}^{-1},\quad f_2 = \sigma_0 n_2 F_{22}^{-1},\ \text{and}\ f_3 = \sigma_0 n_3 F_{33}^{-1} \tag{28}$$

The contact forces in the local reference frame can be obtained from Eq. (28) via the transformation rule:

$$\begin{aligned} {}^g f_n &= \sigma_0[F_{11}^{-1} n_1 n_1 + F_{22}^{-1} n_2 n_2 + F_{33}^{-1} n_3 n_3] \\ {}^g f_s &= \sigma_0[F_{11}^{-1} n_1 s_1 + F_{22}^{-1} n_2 s_2 + F_{33}^{-1} n_3 s_3] \\ {}^g f_t &= \sigma_0[F_{11}^{-1} n_1 t_1 + F_{22}^{-1} n_2 t_2 + F_{33}^{-1} n_3 t_3] \end{aligned} \tag{29}$$

where ${}^g f_n$ is the local contact force along the contact normal (i.e. **n**-direction), and ${}^g f_s$ and ${}^g f_t$ are the tangential contact forces in two tangential directions (i.e. **s**- and **t**-directions). The inverse of the fabric tensor, F_{ij}^{-1}, can be decomposed into two parts:

$$F_{ij}^{-1} = \overline{F}_a \begin{bmatrix} 1 & 0 & 0 \\ 0 & 1 & 0 \\ 0 & 0 & 1 \end{bmatrix} + \overline{F}_b \begin{bmatrix} 0 & 0 & 0 \\ 0 & 0 & 0 \\ 0 & 0 & 1 \end{bmatrix} \tag{30}$$

where $\overline{F}_a = 5(3-a_0)/\rho_c d_g(5-3a_0)$, $\overline{F}_b = -20a_0(3-a_0)/\rho_c d_g(5-3a_0)(5+a_0)$, and a_0 is the degree of fabric anisotropy in the isotropic stress condition. By substituting Eqs. (1) and (30) into (29), the local contact forces can be expressed as:

$$\begin{aligned} {}^g f_n &= \overline{F}_a \sigma_0 + \overline{F}_b \sigma_0 \cos^2\gamma \\ {}^g f_s &= -\overline{F}_b \sigma_0 \cos\gamma \sin\gamma \\ {}^g f_t &= 0 \end{aligned} \tag{31}$$

Thus, the normal elastic contact stiffness in Eq. (19) becomes

$${}^g k_n^{el} = c_n^{el}(\overline{F}_a \sigma_0 / f_{ref})^{\alpha_n^{el}} \left(1 + (\overline{F}_b / \overline{F}_a)\cos^2\gamma\right)^{\alpha_n^{el}} \tag{32}$$

Assuming that the term of $(\overline{F}_b / \overline{F}_a)\cos^2\gamma$ can be ignored, the local contact stiffnesses can be simplified as:

$${}^g k_n^{el} = c_n^{el}(\overline{F}_a \sigma_0 / f_{ref})^{\alpha_n^{el}} \ \text{and}\ {}^g k_r^{el} = c_r^{el}\, {}^g k_n^{el} \tag{33}$$

The elastic contact stiffness matrix in the global coordinate is given by

$$\begin{aligned} K_{ij}^{el} &= {}^g k_n^{el} n_i n_j + {}^g k_r^{el}(s_i s_j + t_i t_j) \\ &= c_n^{el}(\overline{F}_a \sigma_0 / f_{ref})^{\alpha}[n_i n_j + c_r^{el}(s_i s_j + t_i t_j)] \end{aligned} \tag{34}$$

Substituting Eq. (34) into (17), the approximate solutions of the cross-anisotropic elastic moduli and Poisson's ratios in the isotropic stress condition can be derived as follows:

$$E_v^{el} = c_n^{el} c_r^{el}\left[\frac{7d_g^2\rho_c(5+a_0)^2}{5(3-a_0)\{14-2a_0+c_r^{el}(21+9a_0)\}}\right]\left[\frac{5(3-a_0)}{\rho_c d_g f_{ref}(5-3a_0)}\right]^{\alpha_n^{el}}(\sigma_0)^{\alpha_n^{el}} \tag{35a}$$

$$E_h^{el} = c_n^{el} c_r^{el}\left[\frac{7d_g^2\rho_c(5-3a_0)^2}{5(3-a_0)\{14-6a_0+c_r^{el}(21-15a_0)\}}\right]\left[\frac{5(3-a_0)}{\rho_c d_g f_{ref}(5-3a_0)}\right]^{\alpha_n^{el}}(\sigma_0)^{\alpha_n^{el}} \tag{35b}$$

$$G_{vh}^{el} = c_n^{el} c_r^{el}\left[\frac{7d_g^2\rho_c(5-3a_0)^2(5+a_0)^2}{10(5-a_0)(3-a_0)\left\{\begin{matrix}105-46a_0-23a_0^2 \\ +c_r^{el}(70-24a_0+2a_0^2)\end{matrix}\right\}}\right]\left[\frac{5(3-a_0)}{\rho_c d_g f_{ref}(5-3a_0)}\right]^{\alpha_n^{el}}(\sigma_0)^{\alpha_n^{el}} \tag{35c}$$

$$G_{hh}^{el} = c_n^{el} c_r^{el}\left[\frac{7d_g^2\rho_c(5-3a_0)^2}{10(3-a_0)\{21-11a_0+c_r^{el}(14-10a_0)\}}\right]\left[\frac{5(3-a_0)}{\rho_c d_g f_{ref}(5-3a_0)}\right]^{\alpha_n^{el}}(\sigma_0)^{\alpha_n^{el}} \tag{35d}$$

$$\nu_{vh}^{el} = \frac{(7-a_0)(5+a_0)(1-c_r^{el})}{(5-3a_0)\{14-2a_0+c_r^{el}(21+9a_0)\}} \tag{35e}$$

$$\nu_{hv}^{el} = \frac{(7-a_0)(5-3a_0)(1-c_r^{el})}{(5+a_0)\{14-6a_0+c_r^{el}(21-15a_0)\}} \tag{35f}$$

$$\nu_{hh}^{el} = \frac{(7-5a_0)(1-c_r^{el})}{\{14-6a_0+c_r^{el}(21-15a_0)\}} \tag{35g}$$

It should be noted that the error in the approximate solutions depends on the magnitude of a_0 because we ignored the term, $\overline{F}_b / \overline{F}_a = -4a_0/(5+a_0)$, to produce the normal contact force which is not correlated to the contact orientation. For the case that $\alpha_n^{el} = 0.5$ and $c_r^{el} = 0.824$ (i.e. $c_r^{el} = 2(1-\nu_g)/(2-\nu_g)$ with $\nu_g = 0.3$ for quartz), the ratios between the elastic moduli from approximate solutions and those from Eq. (17) are plotted against the magnitude

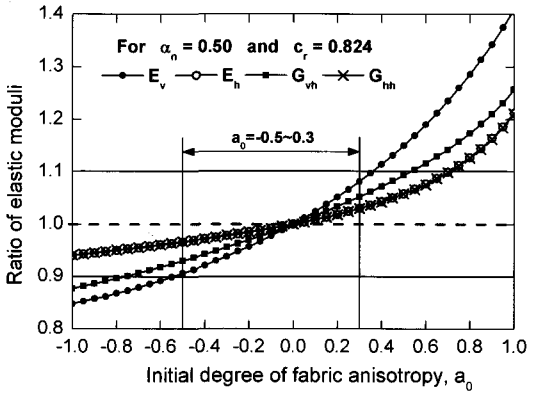

Fig. 5. Variation of $|n-\alpha|$ for the various values of a_1

of a_0 in Fig. 5. As can be seen in Fig. 5, the ratio of elastic moduli ranges between 0.9 and 1.1 for the values of a_0 in between -0.5 and 0.3. When considering the low degree of anisotropy in the isotropic stress and the level of accuracy of measurement in the experiments, such magnitude of errors in the approximate solutions is practically acceptable in the determination of model parameters.

5. Evolution of Contact Orientations

The fabric tensor is manifested in the anisotropic elastic responses in the macroscopic scale. The contact force can be resolved into the component, f^n in the contact normal direction, n_i, and f^r in the tangential direction of the contact plane, r_i, along which the maximum shear contact force applies. In a particular case of the symmetry in the cross-anisotropic material and the triaxial macroscopic stresses, the direction of r_i coincides with the unit vector, s_i so that $f_i = f^n n_i + f^r s_i$. Thus, Eq. (8) can alternatively be expressed as:

$$\sigma_{ij} = \rho_c d_g \left\langle f^n n_i n_j \right\rangle + \rho_c d_g \left\langle f^r s_i n_j \right\rangle \tag{36}$$

By taking the average of normal and tangential contact forces, Eq. (36) becomes,

$$\sigma_{ij} = \rho_c d_g \hat{f}^n \left\langle n_i n_j \right\rangle + \rho_c d_g \hat{f}^r \left\langle s_i n_j \right\rangle = \hat{f}^n F_{ij} \tag{37}$$

where $\hat{f}^n$ and $\hat{f}^r$ are the overall average magnitude of normal and tangential contact forces. Note that $< s_i n_j >= \int_\Omega s_i n_i E(\mathbf{n}) d\Omega = 0$. Consequently, in this limited condition, the macroscopic stress tensor can be proportional to the fabric tensor. Eqs. (4) and (6) allow the explicit relationship between the macroscopic stress and fabric tensor from Eq. (37) such that

$$\begin{bmatrix} \sigma_r & 0 & 0 \\ 0 & \sigma_r & 0 \\ 0 & 0 & \sigma_a \end{bmatrix} = \rho_c d_g \hat{f}^n \begin{bmatrix} \frac{5-3a}{5(3-a)} & 0 & 0 \\ 0 & \frac{5-3a}{5(3-a)} & 0 \\ 0 & 0 & \frac{5+a}{5(3-a)} \end{bmatrix} \tag{38}$$

where $\sigma_r (= \sigma_{11} = \sigma_{22})$ and $\sigma_r (= \sigma_{33})$ denote the radial and axial stresses in the triaxial stress condition, respectively. Furthermore, the mean normal stress, p, and the deviator stress, q, in the triaxial stress condition can be expressed as,

$$p = \frac{\sigma_a + 2\sigma_r}{3} = \frac{\rho_c d_g \hat{f}^n}{3} \quad \text{and} \quad q = \sigma_a - \sigma_r = \frac{4a\rho_c d_g \hat{f}^n}{5(3-a)} \tag{39}$$

Thus, the degree of fabric anisotropy, a, has a unique relationship with the stress ratio, q/p, as:

$$a = \frac{15(q/p)}{12 + 5(q/p)} \tag{40}$$

Despite its mathematical simplicity, Eq. (40) hides some critical points: (i) in general, taking the average of contact forces, especially in the tangential contact direction, is not sufficient to describe the directional variation of the contact force and (ii) Eq. (40) does not allow the anisotropic state of the fabric in the isotropic stress condition. With respect to the directional variation of the contact forces, one can find the enhanced expressions of the stress-contact force-fabric relationship in Mehrabadi et al. (1982) and Ouadfel and Rothenburg (2001). To account for the possible fabric anisotropy in the isotropic stress condition within the simple format of Eq. (40), we modify Eq. (40) as a linear equation:

$$a = a_0 + a_1 (q/p) \tag{41}$$

where a_0 is the magnitude of a in the isotropic stress condition, and a_0 is, in general, the function of contact

Table 1. Required parameters for the micromechanics modeling

Category	Input parameter		Relevant formulation
Contact Stiffness	c_n^{el} and α_n^{el}	Elasticcontact stiffness	${}^g k_n^{el} = c_n^{el} ({}^g f_n / f_{ref})^{\alpha_n^{el}}$
	c_r^{el}		${}^g k_r^{el} = c_r^{el} {}^g k_n^{el}$
	c_n^{ep} and α_n^{ep}	Elastic-plastic contact stiffness	${}^g k_n^{ep} = c_n^{ep} ({}^g f_n / f_{ref})^{\alpha_n^{ep}}$
	c_r^{ep} and α_r^{ep}		${}^g k_r = {}^g c_r^{ep} {}^g k_n^{ep} \left(1 - \frac{{}^g f_r}{{}^g f_n \tan \phi_m}\right)^{\alpha_r^{ep}}$
	ϕ_m		
Contact density	e_0	Initial void ratio	
	d_g	Mean diameter of particles	
Contact orientation	a_0	Initial degree of fabric anisotropy	
	a_1	Evolution of fabric anisotropy	$a = a_0 + a_1 (q/p)$

forces and their directional distribution. The parameter, a_1, relates implicitly to the evolution of contact forces as does the contact force relate to the macroscopic stress in the simplest case of Eq. (40). Herein, a_1 is regarded as a material constant.

6. Conclusions

A micromechanics-based model to simulate the elastic and elastic-plastic behavior of granular soils is developed. The model accounts for the fabric anisotropy represented by the statistical parameter of the spatial distribution of contact normals, the evolution of fabric anisotropy as a function of stress ratio, the continuous change of the co-ordination number relating to the void ratio, and the elastic and elastic-plastic microscopic contact stiffness. The microscopic behavior in a single contact point is thoroughly examined for the various states of contact geometries, which reveals that regardless of contact geometry the normal contact stiffness can be expressed by a power function of the normal contact force. The elastic-plastic contact stiffness is newly derived based on the experimental data for the metallic materials. The elastic-plastic contact stiffness can also be expressed by the power function of the normal contact force as well as the contact force initiating the yielding of contact bodies. To quantitatively assess the microscopic model parameters, the approximate solutions of cross-anisotropic elastic moduli are derived in terms of the micromechanics parameters. The possible errors in the approximation are estimated for the reasonable ranges of the degree of fabric anisotropy. Without the rigorous formulation to describe the evolution of fabric anisotropy, a simple linear relationship between the degree of fabric anisotropy and the stress ratio is provided.

The elastic and elastic-plastic responses in the micromechanical modeling for the nonlinear deformation are meticulously investigated in the companion paper.

Acknowledgements

Financial support for this work was provided by Korea Research Foundation Grant No. KRF-2005-214-D00166. The support of Engineering Research Institute at Seoul National University is greatly appreciated.

References

1. Adams, G. G., and Nosonovsky, M. (2000), "Contact modeling - forces", *Tribology international*, 33, 431-442.
2. Bazant, Z. P., Caner, F. C., Carol, I., Adley, M. D., and Akers, S. A. (2000), "Microplane model M4 for concrete. I: Formulation with work-conjugate deviatoric stress", *Journal of Engineering Mechanics-ASCE*, 126(9), 944-953.

3. Chang, C. S., Chao, S. J., and Chang, Y. (1995), "Estimates of Elastic-Moduli for Granular Material with Anisotropic Random Packing Structure", *International Journal of Solids and Structures*, 32(14), 1989-2008.
4. Chang, C. S., and Gao, J. (1996), "Kinematic and static hypotheses for constitutive modelling of granulates considering particle rotation", *Acta Mechanica*, 115(1-4), 213-229.
5. Chang, C. S., Misra, A., and Sundaram, S. S. (1991), "Properties of granular packings under low amplitude cyclic loading", *Soil Dynamics and Earthquake Engineering*, 10(4), 201-211.
6. Chang, C. S., Sundaram, S. S., and Misra, A. (1989), "Initial Moduli of Particulated Mass with Frictional Contacts", *International Journal for Numerical and Analytical Methods in Geomechanics*, 13(6), 629-644.
7. Christoffersen, J., Mehrabadi, M. M., and Nematnasser, S. (1981), "A Micromechanical Description of Granular Material Behavior", *Journal of Applied Mechanics-Transactions of the Asme*, 48(2), 339-344.
8. Cundall, P. A., and Strack, O. D. L. (1979), "Discrete Numerical-Model for Granular Assemblies", *Geotechnique*, 29(1), 47-65.
9. Darve, F., and Nicot, F. (2005), "On incremental non-linearity in granular media: phenomenological and multi-scale views (Part I)", *International Journal for Numerical and Analytical Methods in Geomechanics*, 29(14), 1387-1409.
10. Einav, I., and Puzrin, A. M. (2004), "Continuous hyperplastic critical state (CHCS) model Derivation", *International Journal of Solids and Structures*, 41(1), 199-226.
11. Emeriault, F., and Cambou, B. (1996), "Micromechanical modelling of anisotropic non-linear elasticity of granular medium", *International Journal of Solids and Structures*, 33(18), 2591-2607.
12. Emeriault, F., and Chang, C. S. (1997), "Interparticle forces and displacements in granular materials", *Computers and Geotechnics*, 20(3-4), 223-244.
13. Fang, H. L. (2003), "A state-dependent multi-mechanism model for sands", *Geotechnique*, 53(4), 407-420.
14. Goddard, J. D. (1990), "Nonlinear Elasticity and Pressure-Dependent Wave Speeds in Granular Media", *Proceedings of the Royal Society of London Series a-Mathematical Physical and Engineering Sciences*, 430(1878), 105-131.
15. Hertz, H. (1882), "Uber die Beruhrung fester elastischer Korper (On the contact of elastic solids)", *Journal of reine und angewandte mathematik*, 92, 156-171.
16. Hicher, P. Y., and Chang, C. S. (2005), "Evaluation of two homogenization techniques for modeling the elastic behavior of granular materials", *Journal of Engineering Mechanics-ASCE*, 131(11), 1184-1194.
17. Jager, J. (1999), "Uniaxial deformation of a random packing of particles", *Archive of Applied Mechanics*, 69(3), 181-203.
18. Johnson, K. L. (1985), *Contact mechanics*, Cambridge University Press, Cambridge.
19. Jung, Y. H., Chung, C. K., and Finno, R. J. (2004), "Development of nonlinear cross-anisotropic model for the pre-failure deformation of geomaterials", *Computers and Geotechnics*, 31(2), 89-102.
20. Kuwano, R., and Jardine, R. J. (2002), "On the applicability of cross-anisotropic elasticity to granular materials at very small strains", *Geotechnique*, 52(10), 727-749.
21. Liao, C. L., Chan, T. C., Suiker, A. S. J., and Chang, C. S. (2000), "Pressure-dependent elastic moduli of granular assemblies", *International Journal for Numerical and Analytical Methods in Geomechanics*, 24(3), 265-279.
22. Liao, C. L., Chang, T. P., Young, D. H., and Chang, C. S. (1997), "Stress-strain relationship for granular materials based on the hypothesis of best fit", *International Journal of Solids and Structures*, 34(31-32), 4087-4100.
23. Love, A. E. H. (1927), *A Treatise of the mathematical theory of elasticity*, Cambridge university press, Cambridge, U.K.
24. Madadi, M., Tsoungui, O., Latzel, M., and Luding, S. (2004), "On the fabric tensor of polydisperse granular materials in 2D", *International Journal of Solids and Structures*, 41(9-10), 2563-2580.
25. Mehrabadi, M. M., Nematnasser, S., and Oda, M. (1982), "On Statistical Description of Stress and Fabric in Granular-Materials", *International Journal for Numerical and Analytical Methods in Geomechanics*, 6(1), 95-108.
26. Mindlin, R. D. (1949), "Comliance of elastic bodies in contact", *Journal of applied mechanics*, 16, 259-270.
27. Mindlin, R. D., and Deresiewicz, H. (1953), "Elastic spheres in contact under varying oblique forces", *Journal of applied mechanics, ASME*, 20(3), 327-344.
28. Mulhearn, T. O. (1959), "Deformation of metals by Vickers-type pyramidal indenters", *J. Mech. Physics Solids*, 7, 85-92.
29. Nicot, F., and Darve, F. (2006), "Micro-mechanical investigation of material instability in granular assemblies", *International Journal of Solids and Structures*, 43(11-12), 3569-3595.
30. Oda, M., Nematnasser, S., and Mehrabadi, M. M. (1982), "A Statistical Study of Fabric in a Random Assembly of Spherical Granules", *International Journal for Numerical and Analytical Methods in Geomechanics*, 6(1), 77-94.
31. Ouadfel, H., and Rothenburg, L. (2001), "'Stress-force-fabric' relationship for assemblies of ellipsoids", *Mechanics of Materials*, 33(4), 201-221.
32. Pestana, J. M., Whittle, A. J., and Salvati, L. A. (2002), "Evaluation of a constitutive model for clays and sands: Part I - sand behaviour", *International Journal for Numerical and Analytical Methods in Geomechanics*, 26(11), 1097-1121.
33. Puzrin, A. M., and Burland, J. B. (2000), "Kinematic hardening plasticity formulation of small strain behaviour of soils", *International Journal for Numerical and Analytical Methods in Geomechanics*, 24(9), 753-781.
34. Samuels, L. E., and Mulhearn, T. O. (1956), "The deformation zone associated with indentation hardness impressions", *J. Mech. Physics Solids*, 5, 125-130.
35. Stallebrass, S. E., and Taylor, R. N. (1997), "The development and evaluation of a constitutive model for the prediction of ground movements in overconsolidated clay", *Geotechnique*, 47(2), 235-253.
36. Walton, O. R., and Braun, R. L. (1986), "Viscosity, granular-temperature, and stress calculations for shearing assemblies of inelastic, friction disks", *Journal of rheology*, 30(5), 949-980.
37. Yimsiri, S., and Soga, K. (2000), "Micromechanics-based stress-strain behaviour of soils at small strains", *Geotechnique*, 50(5), 559-571.
38. Yu, P., and Richart, F. E., Jr. (1984), "Stress ratio effects on shear modulus of dry sands", *Journal of Geotechnical Engineering*, 110(3), 331-345.

(received on Jan. 12, 2007, accepted on Mar. 26, 2007)